Published online May 3, 2018

Journal of Environmental Quality SPECIAL SECTION

MICROBIAL WATER QUALITY—MONITORING AND MODELING

Minimizing Virus Transport in Porous Media by Optimizing Solid Phase Inactivation

Salini Sasidharan,* Scott A. Bradford, Jiří Šimůnek, and Saeed Torkzaban

Abstract

The influence of virus type (PRD1 and ΦX174), temperature (flow at 4 and 20°C), a no-flow storage duration (0, 36, 46, and 70 d), and temperature cycling (flow at 20°C and storage at 4°C) on virus transport and fate were investigated in saturated sand-packed columns. The vast majority (84–99.5%) of viruses were irreversibly retained on the sand, even in the presence of deionized water and beef extract at pH = 11. The reversibly retained virus fraction (f_r) was small (1.6×10^{-5} to 0.047) but poses a risk of long-term virus contamination. The value of f_r and associated transport risk was lower at a higher temperature and for increases in the no-flow storage period due to the temperature dependency of the solid phase inactivation. A model that considered advective–dispersive transport, attachment (k_{att}), detachment (k_{det}), solid phase inactivation (μ_s), and liquid phase inactivation (μ_l) coefficients, and a Langmuirian blocking function provided a good description of the early portion of the breakthrough curve. The removal parameters were found to be in the order of $k_{att} > \mu_s >> \mu_l$. Furthermore, μ_s was an order of magnitude higher than μ_l for PRD1, whereas μ_s was two and three orders of magnitude higher than μ_l for ΦX174 at 4 and 20°C, respectively. Transport modeling with two retention, release, and inactivation sites demonstrated that a small fraction of viruses exhibited a much slower release and solid phase inactivation rate, presumably because variations in the sand and virus surface roughness caused differences in the strength of adhesion. These findings demonstrate the importance of solid phase inactivation, temperature, and storage periods in eliminating virus transport in porous media. This research has potential implications for managed aquifer recharge applications and guidelines to enhance the virus removal by controlling the temperature and aquifer residence time.

Core Ideas

- Solid phase inactivation is 2–3 orders of magnitude higher than liquid phase inactivation.
- Solid phase inactivation increases with temperature and column storage duration.
- The solid phase inactivation was higher for ΦX174 than PRD1.
- Solid phase inactivation reduced the reversible virus fraction by 1 to 2 orders of magnitude.

J. Environ. Qual.
doi:10.2134/jeq2018.01.0027
Supplemental material is available online for this article.
Received 19 Jan. 2018.
Accepted 2 Apr. 2018.
*Corresponding author (salinis@ucr.edu).

Water reclamation, recycling, and reuse are low-cost, low-emission, and low-energy technologies that have received a great deal of interest in industrialized nations to achieve sustainable water supplies for growing populations (Asano and Levine, 1996). A number of managed aquifer recharge (MAR) operations have been designed to purposely inject or infiltrate rainwater, stormwater, reclaimed water, or water from other aquifers into selected aquifers for storage and later recovery (Dillon et al., 2010; Gordon and Toze, 2003). One of the major risks associated with MAR operations is the presence of microbial pathogens in recovered drinking water and their potential risk to human health (Dillon et al., 2010; NHMRC, 2011; NRMMC–EPHC–NHMRC, 2009). If the groundwater already meets drinking water standards or the recovered water is to be used as drinking water, then the source or recovered water requires a higher level of treatment, which adds considerable expense to MAR operations (Dillon et al., 2010).

A growing body of research is continuously evaluating and validating processes involved in pathogen attenuation in aquifers. Most studies have used laboratory-scale columns packed with clean sand (Sasidharan et al., 2017b; Schijven et al., 2002) or sediment collected from potential MAR sites (Hijnen et al., 2005; Sasidharan et al., 2017a), whereas only a few field-scale studies have been conducted (Page et al., 2015; Pieper et al., 1997; Sidhu et al., 2010). Viruses are generally considered to be the microbial pathogen of greatest risk because of their low infectious dose and potential to travel long distances in the subsurface (Reynolds et al., 2008). Mechanisms that will lead to virus removal during MAR include inactivation in the liquid phase, attachment on the solid surface, and subsequent inactivation on the solid surface (Harvey and Ryan, 2004; Sasidharan et al., 2017a; Schijven and Hassanizadeh, 2000). However, current MAR guidelines only consider liquid phase inactivation as a reliable mechanism to remove viruses (Hannappel et al., 2014; Johnson, 1989; NRMMC–EPHC–NHMRC, 2009). Factors influencing liquid phase inactivation (Keswick et al., 1982; Schijven and Hassanizadeh, 2000) of pathogens in aquifers include temperature (Anders and Chrysikopoulos, 2006;

S. Sasidharan and J. Šimůnek, Dep. of Environmental Sciences, Univ. of California, Riverside, Riverside, CA 92521, USA; S. Sasidharan, CSIRO Land and Water, Glen Osmond, SA 5064, Australia; S. Sasidharan and S. Torkzaban, Flinders Univ., Adelaide, SA 5001, Australia; S.A. Bradford, USDA–ARS, US Salinity Lab., Riverside, CA 92507, USA. Assigned to Associate Editor Hyunjung Kim.

Abbreviations: ASR, aquifer storage and recovery; ASTR, aquifer storage transfer and recovery; BTC, breakthrough curve; DLA, double layer agar; MAR, managed aquifer recharge; PFU, plaque forming unit.

Chrysikopoulos and Aravantinou, 2012; Sasidharan et al., 2017b; Schijven et al., 2016), dissolved oxygen (Jansons et al., 1989), water chemistry (Katzenelson, 1978), and the presence of indigenous microorganisms (van Leeuwen, 1996). It may take months to years to achieve one-log virus removal by liquid phase inactivation depending on the system conditions and virus type (Gordon and Toze, 2003; Page et al., 2012; Toze et al., 2010).

Guidelines for MAR have focused on virus removal by liquid phase inactivation because reversible virus attachment and release can create potential risks for long-term virus transport. The objective of this research is to better understand and quantify factors that minimize the risks from reversible virus attachment and release. In particular, we focus on the role of solid phase inactivation to eliminate the release and transport of infective viruses. Many researchers have reported that virus inactivation is greater in the solid phase than the liquid phase (Bradford et al., 2006; Chu et al., 2001; Pieper et al., 1997; Ryan et al., 2002; Schijven et al., 1999). This has been attributed to strong adhesive forces between negatively charged viruses and positively charged metal oxide surfaces (Harvey and Ryan, 2004). In contrast, several other investigators reported that attached viruses can be protected from solid phase inactivation by the presence of organic matter and clay-sized particles in soils (Liew and Gerba, 1980; Schmoll, 2006; Stagg et al., 1977; Yates et al., 1988). Consequently, the relative importance of solid phase inactivation remains a controversial (or perhaps case-specific) issue. In addition, the amount of virus attachment and inactivation will increase with the residence time because they are kinetic processes (Schijven and Hassanizadeh, 2000). The strength of the adhesive force may increase with residence time (Mondon et al., 2003; Stuart and Hlady, 1995; Vadillo-Rodríguez et al., 2004; Xu and Logan, 2006), and this may further enhance irreversible attachment and solid phase inactivation. The temperature of a MAR operation can also influence the rate of attachment and inactivation. Higher temperatures have been reported to increase attachment by decreasing the energy barrier (Sasidharan et al., 2017b) and increase inactivation by enhancing degradation of the viral genome and conformational changes in proteins associated with host recognition (Harvey and Ryan, 2004).

The microbial water quality of recovered water from MAR operations could be improved by optimizing temperature and storage conditions that promote irreversible virus attachment and solid phase inactivation and thereby decrease costs associated with expensive pre- or post-treatment. However, no studies have systematically investigated the influence of temperature and storage time on irreversible attachment and solid phase inactivation under conditions that are relevant for MAR. In addition, the temperature of groundwater can fluctuate with seasonal variations in groundwater recharge and flow (Gunawardhana et al., 2009). This has an important implication on virus survival during the aquifer storage period and on potential health risks associated with active viruses being released into the recovered water. To date, no research has investigated the effect of temperature cycling on reversible–irreversible virus attachment, solid phase inactivation, release during transient chemistry, and the long-term (2–3 mo) virus infectivity during transport experiments.

The objective of this research was to experimentally and theoretically investigate the influence of virus type, temperature, temperature cycling, and storage duration on the extent and kinetics of reversible–irreversible virus attachment and solid phase inactivation. For this purpose, PRD1 and ΦX174 viruses were used in saturated transport (deposition, storage, and release) experiments under different temperatures (4 and/or 20°C), no-flow storage durations (0, 36, 46, and 70 d), and temperature cycling (flow at 20°C and storage at 4°C) conditions. A mass balance was conducted to quantify reversible and irreversible virus fractions. Numerical modeling of the observed breakthrough curves (BTCs) was used to inversely determine the rates of attachment, detachment, and solid phase inactivation. Results from this work provide valuable insight into the underlying mechanisms that control the transport and fate of viruses, as well as the design of MAR operations to eliminate viruses by solid phase inactivation.

Materials and Methods

Porous Medium and Electrolyte Solution

Ultrapure quartz sand (Charles B. Chrystal Co., Inc.) with size ranging from 125 to 300 μm was used in transport experiments. The sand was cleaned using an acid wash and boiling procedure described by Sasidharan et al. (2014). An electrolyte solution of 10 mM was prepared for transport studies using analytical grade NaCl and Milli-Q water at unadjusted pH of 5.5 to 5.8 as in previous studies (Walker et al., 2004; Zhang et al., 2010).

Viruses

Bacteriophages PRD1 and ΦX174 were used as the model viruses in this study. The bacteriophages were analyzed using their respective *Escherichia coli* host. The characteristics of these viruses, their production, and quantification using the double layer agar (DLA) method are described in Sasidharan et al. (2016). The detection limit of the DLA technique is around 30 plaque forming unit (PFU) mL^{-1} (ISO, 2000). Stock solutions of viruses were diluted in the electrolyte solution and equilibrated at the experimental temperature (4 or 20°C). An average input concentration (C_0) of 3.98×10^6 PFU mL^{-1} for PRD1 and 7.17×10^5 PFU mL^{-1} for ΦX174 were used. The liquid phase inactivation rate of PRD1 and ΦX174 was determined over a period of 70 d in 10 mM NaCl at 4 and 20°C.

Transport Experiments

The column experiments were conducted in temperature-controlled laboratories (4 ± 1 and 20 ± 1°C). Sterilized polycarbonate columns (1.9 cm i.d. and 5 cm height) were wet-packed using clean quartz sand while the column was being vibrated. The packed column has a porosity of 0.4. After packing, the column was preconditioned with 10 pore volumes of a 10 mM NaCl solution using a syringe pump (Model 22, Harvard Apparatus) at a pore-water velocity of 5 m d^{-1}. The columns were equilibrated to the selected temperature (4 and 20°C) for 12 h before starting the experiment. The virus transport experiments consisted of a deposition phase (Phase I), a storage phase (Phase II), and four release phases (Phases III–VI). A virus (PRD1 or ΦX174) suspension in 10 mM NaCl solution at a temperature of 4 or 20°C was introduced into the column at an average pore-water velocity of 0.1 m d^{-1} during Phase I. Various storage periods and temperatures were implemented during Phase II that are discussed in the following paragraph. Phase III consisted of eluting the column with

virus-free 10 mM NaCl solution at a pore-water velocity of 0.1 m d^{-1}. Columns were eluted with Milli-Q water and beef extract with pH 11 (Sasidharan et al., 2017a) during Phases IV and V, respectively, at a pore-water velocity of 5 m d^{-1}. The column effluent samples were collected using a Spectra/Chrom CF-1 Fraction Collector (Spectrum), and the concentration of viruses was quantified using the DLA method (Sasidharan et al., 2016).

Three sets of virus transport experiments were conducted to mimic different MAR strategies and to better differentiate between liquid phase inactivation, reversible and irreversible attachment on the solid phase, and solid phase inactivation. The first set of experiments did not implement a storage period during Phase II. These experiments focused on the influence of constant temperature conditions (4 or 20°C) on virus transport and release. The second set of experiments included a storage period of 0, 46, or 70 d during Phase II to study the effects of solid phase inactivation under constant temperature conditions (4 or 20°C). A 70-d storage period was used for comparison to field-scale pathogen decay studies (Sidhu et al., 2015) and to investigate the worst-case (minimum) residence time scenario (when winter, spring, and summer storms are harvested) during MAR. Columns were closed, wrapped within thin aluminum foil sheets, and stored under constant temperature conditions during this storage period. The third set of experiments implemented temperature cycling and a storage period by conducting Phases I and III to VI at 20°C and Phase II at 4°C with a storage period of 0, 36, 46, or 70 d. These experiments were designed to study the influence of seasonal variations in temperature on solid phase inactivation.

Following completion of Phases I to V, the quartz sand from the column was decanted into a test tube and washed with 10 mL pH 11 solution twice, and the eluted virus concentration was determined using the DLA method (Phase VI). In addition, spot tests were conducted after completion of Phases I to VI for the storage at constant temperature experiments to determine whether remaining viruses on the solid phase were still capable of infecting and reproducing on their host bacterium. First, 5 g of washed (pH = 11) quartz sand was incubated with 25 mL of Tryptone Soy Broth (Oxoid, Thermo Scientific, CM0129) and the *E. coli* hosts (separate flasks for each host) at 37°C for 12 h. The broth was collected, 2.5 mL of chloroform was added to the broth, and the broth was stored in the refrigerator overnight. The aqueous phase was centrifuged at 3000 × *g* for 20 min and the supernatant was collected. The spot test was conducted as follows. One milliliter of *E. coli* host grown to the log phase was mixed with 40 mL of Tryptone Soy agar (Oxoid, Thermo Scientific, CM0131) that had 10 mM $CaCl_2$, poured into a Petri dish, and allowed to dry completely. Next, 10 μL of virus supernatant was placed onto the Petri dish as a spot (seven spots in total), allowed to dry completely, and incubated at 37°C overnight. The plates were observed for the presence of spots (i.e., clear/lysis zone or plaques).

The observed BTCs were plotted as a dimensionless concentration (C/C_0) of viruses as a function of pore volumes. The total mass of retained viruses during Phase I (M_S) in the column experiment was determined by calculating the difference between the mass of injected viruses into the column in Phase I (M_{In}) and the mass of viruses that was recovered in the effluent BTC (M_{BTC}) during Phase I. The percentage of injected viruses that was recovered during Phases III, IV, V, and VI were denoted as M_{III}, M_{IV}, M_V, and M_{VI}, respectively. The percentage of the total mass of the viruses recovered ($M_{III} + M_{IV} + M_V + M_{VI}$) was denoted as M_R. The percentage of injected viruses that were irreversibly retained on the solid phase (M_{Irr}) was determined as $100 - M_{BTC} - M_R$. The total fraction of the viruses that were released from M_S ($f_r = M_R/M_S$) and the total fraction of viruses that were not released from M_S ($f_{nr} = M_{Irr}/M_S$) were also calculated.

Mathematical Modeling

Experimental BTCs for viruses were simulated by numerically solving the following aqueous phase and solid phase mass balance equations using the HYDRUS-1D model (Šimůnek et al., 2016):

$$\frac{\partial C}{\partial t} = \lambda v \frac{\partial^2 C}{\partial z^2} - v\frac{\partial C}{\partial z} - \left(k_{att1}\psi_1 + k_{att2}\right)C + \frac{\rho_b}{\theta}\left(k_{det1}S_1 + k_{det2}S_2\right) - \mu_l C \quad [1]$$

$$\frac{\rho_b}{\theta}\frac{\partial S_1}{\partial t} = k_{att1}\psi_1 C - \frac{\rho_b}{\theta}(k_{det1} + \mu_{s1})S_1 \quad [2]$$

$$\frac{\rho_b}{\theta}\frac{\partial S_2}{\partial t} = k_{att2} C - \frac{\rho_b}{\theta}(k_{det2} + \mu_{s2})S_2 \quad [3]$$

where t (T; T denotes unit of time) is time, z (L; L denotes units of length) is the direction of mean water flow, C (N L^{-3}; N denotes the virus number) is the aqueous phase virus concentration, λ (L) is the dispersivity, v (L T^{-1}) is the average pore-water velocity, ρ_b (M L^{-3}; M denotes the unit of mass) is the bulk density, θ is the water content, S (N M^{-1}) is the solid phase virus concentration, k_{att} (T^{-1}) is the virus attachment rate coefficient, k_{det} (T^{-1}) is the virus detachment rate coefficient, μ_s (T^{-1}) is the solid phase virus inactivation rate, μ_l (T^{-1}) is the liquid phase virus inactivation rate, and subscripts 1 and 2 on parameters indicates the solid phase sites. The parameter ψ_1 is a dimensionless Langmuirian blocking function that is given as (Adamczyk et al., 1994)

$$\psi_1 = \left(1 - \frac{S_1}{S_{max1}}\right) \quad [4]$$

where S_{max1} (N M^{-1}) is the maximum solid phase concentration of retained virus on Site 1.

Note that the above model considers two kinetic retention and inactivation sites on the solid phase, and Langmuirian blocking only on Site 1. The justification for the selection of this model formation will be given in the "Mathematical Modeling" section under "Results and Discussion." The value of μ_l was calculated from the 70-d liquid phase inactivation study. Other model parameters were determined from available experimental information (e.g., v, θ, ρ_b, λ) or by optimization to the virus BTCs using the nonlinear least squares fitting routine in HYDRUS-1D. The possibility of non-unique parameter fits increases with the complexity of the model and the number of fitted model parameters. Our modeling analysis of the virus transport data was therefore conducted in a stepwise manner to constraint model parameters and to minimize the potential for non-unique parameter fits. Initially, only a one-site retention and

inactivation model was used to describe the early-time portion of the BTC by setting parameters for Site 2 to zero and using the following sequence. In the first step, k_{att1} and S_{max1} were fitted to only the deposition phase (Phase I), and the tailing portion of the BTC was neglected. These values of k_{att1} and S_{max1} were kept as constant during step 2, and k_{det1} and μ_{s1} were fitted to the deposition (Phase I) and the initial tailing portion the BTC. The full two-site model was needed to accurately describe the additional complexity of the long-term portion of the BTC. In step 3, the values of S_{max1}, k_{det1}, and μ_{s1} from step 2 were constants while fitting values of k_{att1}, k_{att2}, k_{det2}, and μ_{s2}.

The fraction of the solid surface area that is available for retention (S_f) was calculated from S_{max1} as follows (Kim et al., 2009; Sasidharan et al., 2014):

$$S_f = \frac{A_c \rho_b S_{max1}}{(1-\gamma)A_s} \quad [5]$$

where A_c ($L^2 N^{-1}$) is the cross-sectional area of a virus, A_s (L^{-1}) is the solid surface geometric area per unit volume, and γ is the porosity of a monolayer packing of viruses on the solid surface that was taken from the literature to be 0.5 (Johnson and Elimelech, 1995).

The value of the sticking efficiency (α) was determined from the fitted $k_{att} = k_{att1} + k_{att2}$ value and filtration theory as follows (Schijven and Hassanizadeh, 2000; Yao et al., 1971):

$$\alpha = \frac{2 d_c k_{att}}{3(1-n) v \eta} \quad [6]$$

where n is the porosity (0.4) and d_c (L) is the collector (median grain) diameter. The value of the single collector-efficiency, η, was calculated using the correlation equation presented by Messina et al. (2015).

Results and Discussion

Liquid Phase Virus Inactivation

Table 1 shows the calculated first-order liquid phase inactivation coefficient (μ_l) for PRD1 and ΦX174 in 10 mM NaCl at 4 and 20°C over a 70-d period. The result shows that the liquid phase inactivation increased for ΦX174 in comparison to PRD1. Furthermore, the value of μ_l was 121 and 388% higher at 20°C than at 4°C for viruses PRD1 and ΦX174, respectively. Field-scale pathogen decay studies at MAR site (average temp = 23–25°C) using human pathogenic viruses showed ~109 to 185 d for 1 log removal of viruses (Sidhu et al., 2015). Hence, human pathogenic viruses and the bacteriophages used in this study exhibited similar decay rates. Viruses are submicron to nanosized particles that contain genetic materials (nucleic acid) such as RNA or DNA surrounded by a protein coat capsid. The major mechanisms in viral inactivation are nucleic acid degradation, loss of nucleic acid, fracture of the capsid protein, and loss of host reorganization sites, which will lead to their complete degradation and/or loss of infectivity (Harvey and Ryan, 2004). Previous researchers demonstrated that temperature plays a dominant role in liquid phase virus inactivation (Blanc and Nasser, 1996; Harvey and Ryan, 2004; Schijven et al., 2016).

The relatively low values of R^2 for μ_l in Table 1 reflect a deviation from the first-order model and scatter in the data. To overcome this limitation, previous studies used different models to simulate liquid phase inactivation. Sim and Chrysikopoulos (1996), for example, used a time-dependent inactivation model to account for virus subpopulations with different inactivation rates. We did not investigate this issue further here because results shown below demonstrated that liquid phase inactivation had an insignificant influence in our column-scale studies.

Virus Transport Experiments

Figure 1 presents breakthrough and release curves for PRD1 and ΦX174 under constant temperature conditions of 4 and 20°C. Table 2 shows mass balance data for the virus breakthrough and release curves. Similar to Sasidharan et al. (2016), the retention of viruses was higher at 20 than at 4°C, and for ΦX174 than PRD1. For example, the mass retained on the solid phase (M_S) for PRD1 and ΦX174 was 90.6 and 99.2% at 20°C compared with 88.1 and 98.9%, respectively, at 4°C. The release of PRD1 and ΦX174 was initiated during Phases III (~51 d of virus-free 10 mM NaCl solution at 0.1 m d^{-1}), IV (Milli-Q water at 5 m d^{-1}), and V (beef extract with pH 11 at 5 m d^{-1}) at 4 and 20°C. Figure 1 shows that only a small number of the injected viruses were released (<4.17%) during Phases III, IV, and V at both 4

Table 1. A summary of the experimental condition (temperature) and model parameters that were fitted to the viruses PRD1 and ΦX174 breakthrough curves using one-site and two-site kinetic models (the attachment coefficient, k_{att}; the detachment coefficient, k_{det}; the maximum solid phase virus concentration, S_{max}/C_0; and solid phase inactivation, μ_s). The subscripts 1 and 2 represent the first and second sites, respectively. The parameters α, S_f, and η were calculated from k_{att}, S_{max}/C_0, and the correlation equation of Messina et al. (2015), respectively. The table also includes the coefficient of determination (R^2) for the goodness of model fit and liquid phase inactivation coefficient, μ_l. All experiments were conducted at temperature = 4 or 20°C, ionic strength = 10 mM NaCl, and flow velocity = 0.1 m d^{-1}. Observed and simulated breakthrough curves are shown in Fig. 1B.†

Virus	Temp.	Model	k_{att1}	k_{det1}	S_{max1}/C_0	μ_{s1}	k_{att2}	k_{det2}	R^2 (Model)	S_f	α	η	μ_l	R^2 (μ_l)
	°C		min^{-1}	min^{-1}	no. g^{-1}	min^{-1}	min^{-1}	min^{-1}					min^{-1}	
ΦX174	4	one-site	1.5×10^{-2}	4.9×10^{-5}	0.763	4.7×10^{-4}	NA‡	NA	0.65	7.8×10^{-9}	0.031	0.65	2.2×10^{-6}	0.37
		two-site	1.1×10^{-2}				4.3×10^{-4}	1.2×10^{-6}	0.62					
	20	one-site	1.2×10^{-2}	4.9×10^{-4}	0.953	1.5×10^{-3}	NA	NA	0.50	9.8×10^{-9}	0.028	0.71	8.6×10^{-6}	0.87
		two-site	1.1×10^{-2}				7.6×10^{-5}	4.8×10^{-7}	0.68					
PRD1	4	one-site	1.4×10^{-2}	5.0×10^{-4}	0.46	5.9×10^{-4}	NA	NA	0.70	1.6×10^{-7}	0.049	0.54	1.3×10^{-6}	0.37
		two-site	1.5×10^{-2}				4.0×10^{-5}	9.2×10^{-7}	0.71					
	20	one-site	2.5×10^{-2}	4.8×10^{-8}	2.43	4.2×10^{-5}	NA	NA	0.76	8.5×10^{-7}	0.081	0.60	1.6×10^{-6}	0.28
		two-site	2.8×10^{-2}				1.0×10^{-7}	1.0×10^{-12}	0.77					

† Note that the fitted values of μ_{s2} were always less than 1.0×10^{-12}.

‡ NA, not applicable. The parameter is not fitted during the simulation.

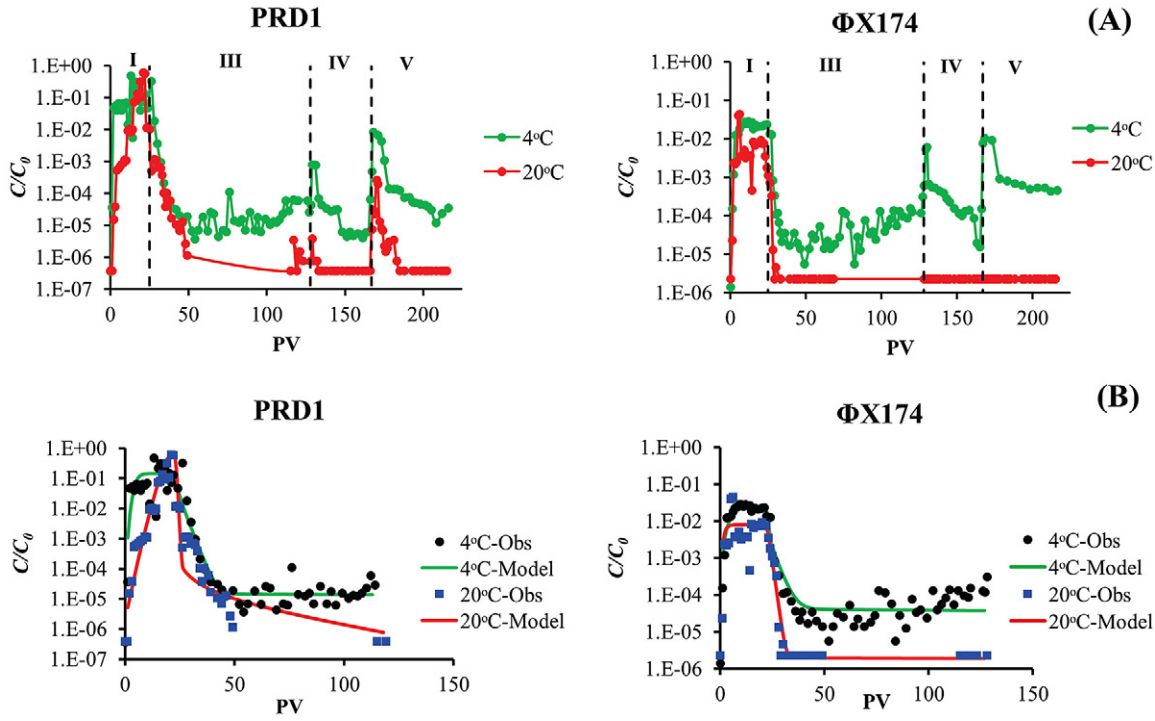

Fig. 1. (A) The observed breakthrough curve for viruses PRD1 and ΦX174 for the experiments conducted at temperature = 4 and 20°C, ionic strength = 10 mM NaCl, and flow velocity = 0.1 m d^{-1}. (B) The observed (markers) and fitted (solid line) breakthrough curve for viruses PRD1 and ΦX174 for Phase I and Phase III. C/C_0, output concentration/input concentration; PV, pore volume. Table 1, Supplemental Table S1, and Table 2 present fitted model parameters, standard error coefficient, and mass balance information, respectively.

and 20°C, even in the presence of Milli-Q water (Phase IV) or especially beef extract at pH = 11 (Phase V), which produced higher release peak concentrations. Similarly, mass balance information (Table 2) indicates that 95 to 99% of the injected viruses remained irreversibly attached or inactivated on the solid surface. However, virus release was greater for PRD1 than ΦX174 and at 4 than 20°C; this suggests a potential transport risk for some viruses at lower temperatures.

One way to potentially minimize the risk from virus transport during MAR operations such as aquifer storage and recovery (ASR) and aquifer storage transfer and recovery (ASTR) is to provide an adequate residence time for liquid and especially solid phase inactivation. Additional transport experiments with PRD1 and ΦX174 at constant temperatures of 4 and 20°C were therefore conducted to investigate the influence of different storage periods before initiating release during Phases III, IV, and V. Figures 2A and 2B present breakthrough and release curves for PRD1 and ΦX174 at 4°C with a storage time of 0 or 70 d. Figures 2C and 2D present similar results for PRD1 and ΦX174 at 20°C when a 0- and 70-d storage period was implemented. Table 2 summarizes experimental conditions and mass balance data during these experiments. An increase in the storage period lowered the effluent virus concentrations during the release Phases III, IV, and V. The difference in effluent concentration with storage time was greater for ΦX174 than PRD1 and for 20 than 4°C, due to differences in solid phase inactivation. Similarly, the reversible virus fraction was reduced by one to two orders of magnitude when the storage period was increased, a drop that was enhanced at higher temperatures. These results demonstrate that immediate release does not give adequate time for solid phase inactivation. In contrast, longer storage periods can significantly contribute to virus removal by solid phase inactivation, especially at higher temperatures. Indeed, the value of C/C_0 was below the detection limit for ΦX174 at 20°C during all release phases following a 70-d storage period. Consequently, a lower storage time is needed at a higher temperature because of an increase in the solid phase inactivation. However, solid phase inactivation over a 70-d storage period can still contribute to a one order of magnitude reduction in a reversible virus fraction even under a worst-case scenario of PRD1 at 4°C.

Following completion of the virus transport and storage experiments shown in Fig. 2, sand samples from the columns were collected, washed twice with pH 11 solution, and then analyzed for infective virus concentrations using the spot test procedure described in section "Transport Experiments" under "Materials and Methods" above. The sand from transport and storage experiments at 4 and 20°C after 0 d was positive (presence of a few PFUs) for the PRD1 virus. This indicates that some of the irreversibly retained viruses were still infectious on the solid surface under these conditions. In contrast, sand from experiments at 20°C was negative (no PFU) for PRD1 after 70 d, and negative for ΦX174 after 0 and 70 d. However, both ΦX174 and PRD1 were positive (a few PFUs) at 4°C after 0 and 70 d of storage period. This provides convincing evidence that given sufficient storage time, irreversibly attached viruses can be inactivated on the solid phase at a higher temperature. However, the lower temperature conditions need more time for complete solid phase inactivation and may pose a health risk, and therefore, the temperature effect should be taken into account in MAR designs.

Seasonal temperature variations initiate and drive thermal groundwater convection, especially during the transition from summer to winter months (Engström and Nordell, 2016). In natural systems, thermally driven convection is initiated by various processes such as varying groundwater flow and infiltration of rain and

snowmelt water, which may lead to a decline in groundwater temperature. Such changes in groundwater temperature will influence the amounts of virus retention and inactivation (Fig. 1). The next set of ΦX174 and PRD1 transport experiments, therefore, investigated the combined influence of temperature cycling and storage period. In particular, Phases I, III, IV, and V were all conducted at 20°C. Virus release was initiated immediately following Phase I in some experiments (storage period of 0 d), whereas others were subjected to a 36-, 46-, or 70-d storage period at 4°C before initiating release at 20°C. Figure 3 presents the breakthrough and release curves for these temperatures cycling and storage experiments. Table 2 presents a summary of the experimental conditions and mass balance data. Similar to constant temperature storage experiments (Fig. 2, Table 2), Fig. 3 and Table 2 revealed small amounts of virus release and that the reversible virus fraction decreased for longer storage periods and for ΦX174 in comparison to PRD1. However, temperature cycling and storage experiments show intermediate release behavior to the storage experiments that were conducted at a constant temperature of 4 or 20°C (Fig. 2, Table 2). The temperature cycling and storage study, therefore, confirms that the solid phase inactivation is a function of temperature and that the required storage period to remove viruses by solid phase inactivation will need to account for temperature fluctuations.

Mathematical Modeling

Mathematical modeling of ΦX174 and PRD1 transport during Phases I and III was undertaken to better understand and quantify the relative importance of different processes at 4 and 20°C. Initially, the virus breakthrough curves shown in Fig. 1 were modeled using only a one-site kinetic retention model that included Langmuirian blocking and liquid and solid phase inactivation. Blocking was included in the model because some breakthrough curves exhibited a delay in breakthrough and then an increase in the effluent virus concentration with continued injection due to the filling of available retention sites. Fitted (k_{att1}, k_{det1}, S_{max1}, and μ_{s1}), measured (μ_l), and calculated (α, η, and S_f) model parameters, as well as statistical measures of the goodness of fit, are provided in Table 1. The standard error coefficients for fitted parameters are given in Supplemental Table S1.

The one-site model captured the main processes controlling the early portion of the breakthrough curve. Fitted (k_{att1} and S_{max1}) and calculated (η and S_f) retention parameters were higher with increasing temperature. Sasidharan et al. (2017b) previously attributed this temperature dependency to slight increases in the adhesive interaction on heterogeneous surfaces and slight differences in mass transfer (η in Table 1). Similar to Sasidharan

Table 2. The mass balance information for viruses column experiments shown in Fig. 1, 2, and 3.

Figure	Virus	Temp.	Storage period	Retention†				Release‡					
				M_{BTC}	M_S	M_{Irr}	f_{nr}	f_r	M_{III}	M_{IV}	M_V	M_{VI}	M_R
		°C	d	%				%					
Fig. 1A	PRD1	20	0	9.4	90.61	90.4	0.998	0.001	0.18	1.1×10^{-4}	2.9×10^{-3}	1.9×10^{-4}	0.18
		4		11.8	88.14	84	0.953	0.047	3.9	0.02	0.25	6.4×10^{-4}	4.17
	ΦX174	20		0.8	99.18	99.2	0.999	1.1×10^{-4}	0.01	4.0×10^{-4}	5.1×10^{-4}	0	0.01
		4		1	98.99	98.6	0.997	0.004	0.14	0.05	0.24	0.01	0.44
Fig. 2A	PRD1	4	0	8.6	91.38	89.37	0.980	0.02	1.42	0.44	0.13	0.01	2.0
			70	10.1	89.87	89.53	0.995	0.003	0.03	0.19	0.11	1.5×10^{-3}	0.3
Fig. 2B	ΦX174		0	1.79	98.21	96.40	0.982	0.018	0.15	0.2	0.88	0.58	1.81
			70	1.99	98.01	97.19	0.992	0.008	0.29	0.37	0.16	7.4×10^{-4}	0.82
Fig. 2C	PRD1	20	0	0.8	99.20	98.73	0.995	0.004	0.09	0.10	0.26	5.7×10^{-3}	0.47
			70	4.6	95.44	95.44	1	2.1×10^{-5}	0.002	3.9×10^{-4}	4.5×10^{-4}	1.6×10^{-4}	0.003
Fig. 2D	ΦX174		0	0.03	99.97	99.14	0.992	0.008	0.001	0.03	0.78	0.02	0.83
			70	0.55	99.44	99.44	1	1.6×10^{-5}	2.4×10^{-4}	4.6×10^{-4}	5.5×10^{-4}	5.6×10^{-4}	0.001
NA§	PRD1	20	0	5.37	94.63	92.45	0.977	0.02	1.07	0.19	0.89	0.005	2.17
			46	7.0	93.00	92.36	0.993	0.007	0.63	1.6×10^{-4}	2.9×10^{-4}	6.5×10^{-4}	0.64
	ΦX174		0	0.11	99.89	99.41	0.995	0.004	0.03	0.07	0.35	0.06	0.48
			46	0.73	99.27	99.25	0.999	2.0×10^{-4}	0.02	9.7×10^{-5}	1.1×10^{-4}	0	0.02
Fig. 3A	PRD1	$20–4_{Storage}–20$	0	5.37	94.63	92.45	0.977	0.02	1.07	0.19	0.89	0.005	2.17
			36	6.57	93.43	92.57	0.991	0.009	0.85	2.7×10^{-4}	3.8×10^{-4}	5.4×10^{-4}	0.86
			46	7.08	92.92	92.11	0.992	0.009	0.79	2.5×10^{-3}	8.1×10^{-3}	8.3×10^{-4}	0.81
Fig. 3B	ΦX174		0	0.11	99.89	99.41	0.995	0.004	0.03	0.07	0.35	0.06	0.48
			36	0.54	99.46	99.33	0.999	0.001	0.12	2.4×10^{-3}	4.7×10^{-3}	0	0.13
			46	0.37	99.63	99.57	0.999	6.0×10^{-4}	0.05	1.2×10^{-4}	7.3×10^{-5}	0	0.05
Fig. 3C	PRD1		0	0.8	99.20	98.73	0.995	0.004	0.09	0.10	0.26	5.7×10^{-3}	0.47
			70	4.5	95.49	95.43	0.999	6.1×10^{-4}	0.003	0.04	0.2	5.2×10^{-4}	0.06
Fig. 3D	ΦX174		0	0.03	99.97	99.14	0.992	0.008	0.001	0.03	0.78	0.02	0.83
			70	0.55	99.45	99.38	0.999	7.1×10^{-4}	0.001	0.02	0.04	0.003	0.07

† M_{BTC}, mass of viruses recovered in the effluent breakthrough curve (BTC); M_S, total mass of retained viruses during Phase I; M_{Irr}, percentage of injected viruses irreversibly retained on the solid phase.

‡ M_{III}, M_{IV}, M_V, and M_V, percentage of injected viruses recovered during Phases III, IV, V, and VI, respectively; M_R, percentage of the total mass of the viruses recovered ($M_{III} + M_{IV} + M_V + M_{VI}$).

§ NA, not applicable. These data are not presented as a figure in the text.

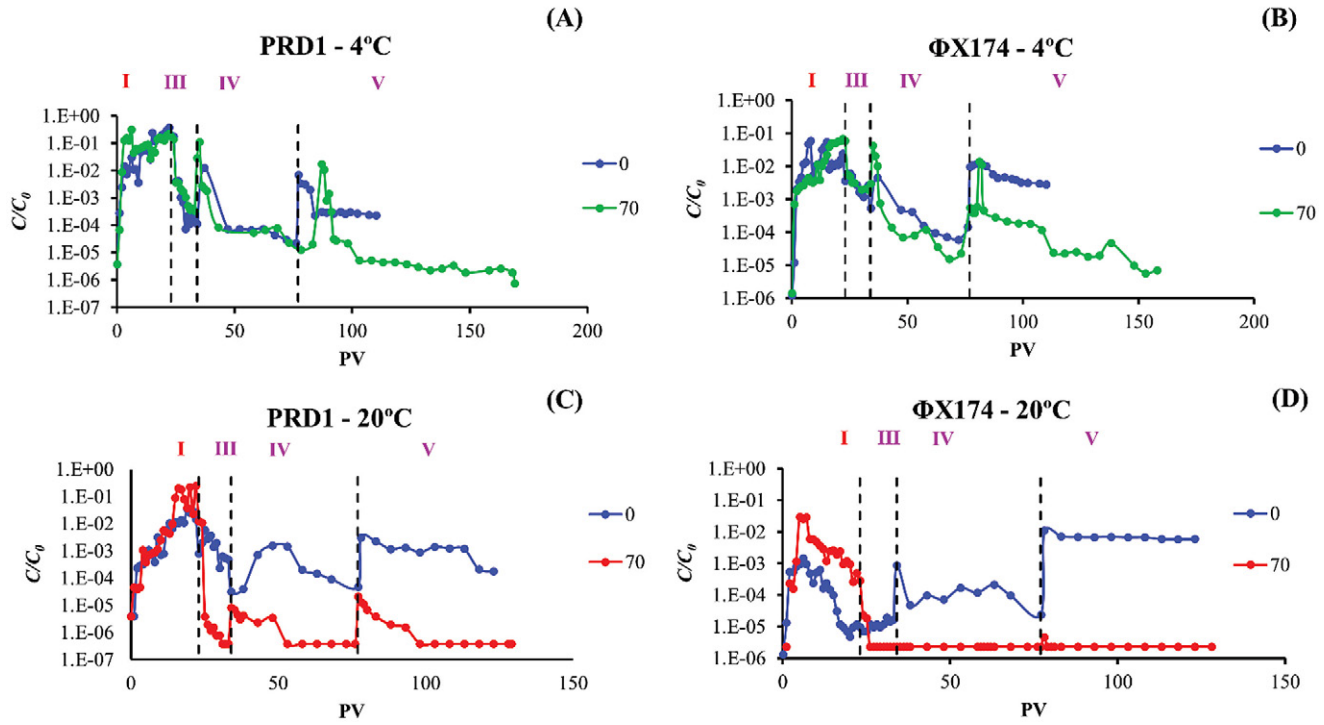

Fig. 2. The observed breakthrough curves for viruses PRD1 and ΦX174 at temperature = 4 and 20°C, ionic strength = 10 mM NaCl, and flow velocity = 0.1 m d^{-1}. The release phases (Phases III, IV, and V) were conducted either immediately after the retention phase or after storing the columns for 70 d under the respective experimental temperature. (A) PRD1 and (B) ΦX174 at 4°C, and (C) PRD1 and (D) ΦX174 at 20°C. C/C_0, output concentration/input concentration; PV, pore volume. Table 2 shows the corresponding mass balance data.

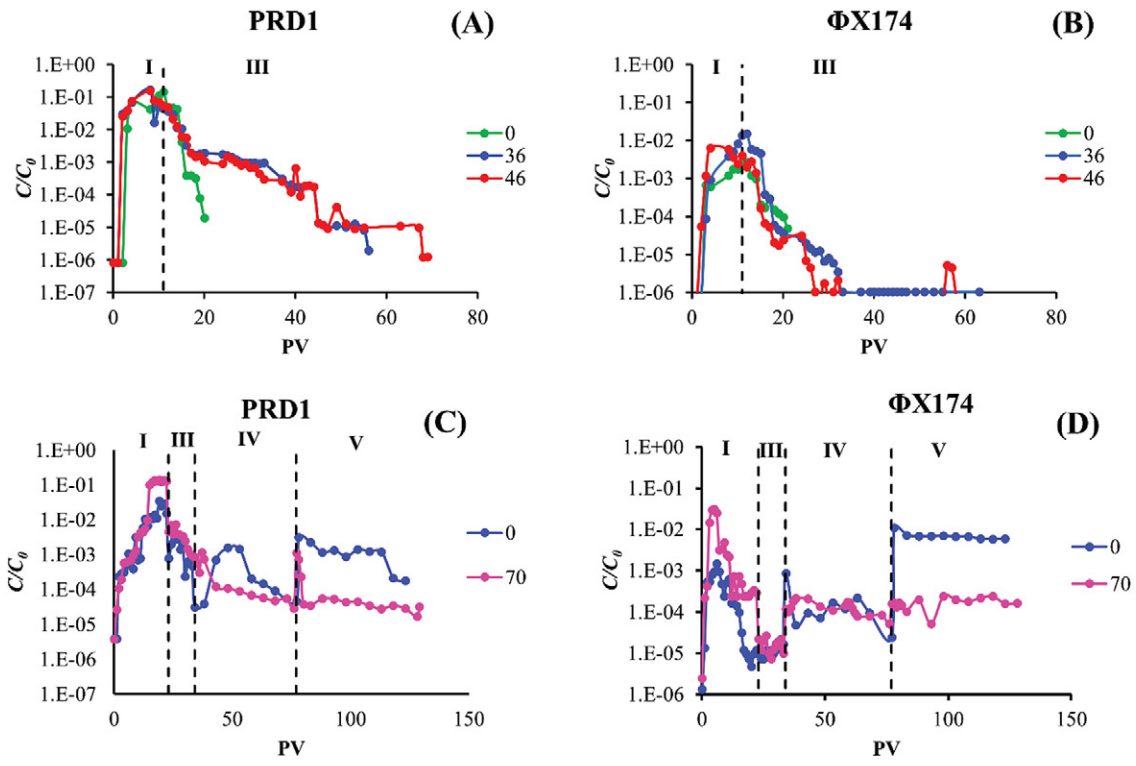

Fig. 3. The observed breakthrough curve for viruses PRD1 and ΦX174 at ionic strength = 10 mM NaCl, flow velocity = 0.1 m d^{-1}, and temperature = 20°C. The first set of columns were released immediately after the retention phase (Phase I). Remaining columns were stored at 4°C (Phase II) and the release phases (Phases III, IV, and V) were conducted after various storage durations. (A) PRD1 and (B) ΦX174 after 0, 36, or 46 d of storage. (C) PRD1 and (D) ΦX174 after 0 and 70 d of storage. Phases III, IV, and V were conducted at temperature = 20°C and flow velocity = 5 m d^{-1} using the following solution chemistry: Phase III = 10 mM NaCl, Phase IV = Milli-Q water, and Phase V = beef extract with pH 11. C/C_0, output concentration/input concentration; PV, pore volume. The corresponding mass balance data is given in Table 2.

et al. (2017a), it was found that $k_{att1} > \mu_{s1} >> \mu_l$. Significantly, μ_{s1} was two and one orders of magnitude higher than μ_l for PRD1, whereas μ_{s1} was two and three orders of magnitude higher than μ_l for ΦX174 at 4 and 20°C, respectively. Generally, the inactivation parameters μ_{s1} and μ_l were higher with increasing temperature and for ΦX174 than PRD1 (Tables 1 and 2). The standard error coefficients on fitted one-site parameters were generally low but were somewhat higher for some parameter (k_{att1} and S_{max1}) associated with ΦX174 at 20°C because of uncertainty in blocking.

Calculations shown in Table 2 indicate that a small fraction of the injected virus was reversibly retained and not inactivated (<4.17%), and the remaining fractions were irreversibly retained or inactivated on the solid phase. The one-site retention model did not account for the reversible virus fraction that was not inactivated, and therefore this model could not provide an accurate description of the observed low concentration tailing that poses an important long-term transport risk of viruses in MAR systems. To account for this behavior, a model with two kinetic retention sites and separate solid phase inactivation rates was needed. The simulated breakthrough curves for this two-site model are shown in Fig. 1B. Fitted model parameters and a statistical measure of the goodness of fit are shown in Table 1. Standard error coefficients for fitted parameters are given in Supplemental Table S1. Note that $k_{att1} >> k_{att2}$, $\mu_{s1} >> \mu_{s2}$, and $k_{det1} > k_{det2}$. This suggests that attached viruses on Site 2 detach at a smaller rate than Site 1 and a very small fraction of these viruses was inactivated at a much slower rate on Site 2 than on Site 1. The standard error coefficient for some fitted two-site model parameters was high (Supplemental Table S1) due to the increased complexity and parameter uncertainty of this model. Nevertheless, R^2 values between measured and simulated breakthrough curves were always >0.62; this agreement suggests that long-term virus transport and fate processes were correctly captured by the two-site model.

A small fraction of viruses was released at a very small rate during Phases III to V (Tables 1 and 2). This could be explained by the difference in adhesive strength of the viruses at a specific attachment location. Previous studies demonstrated that the presence of nanoscale roughness and chemical heterogeneity on sand (Han et al., 2016; Choo et al., 2015) and virus (Kazumori, 1981; McKenna et al., 1992; Merckel et al., 2005; Peralta et al., 2013) are expected to reduce the magnitude of the energy barrier to attachment/detachment and the depth of the primary minimum (Bradford et al., 2017; Bradford and Torkzaban, 2013, 2015; Torkzaban and Bradford, 2016). The observation of low rates of virus detachment (Table 1) is consistent with slow, diffusion-controlled, virus release from a primary minimum with a low probability of release (e.g., the energy barrier to detachment of 5 to 10 kT) (Bradford et al., 2017). Previous studies demonstrated that a strong adhesive interaction of viruses to a solid surface can lead to structural damage and the leakage of virus genetic material (adsorption of influenza virus on the hydrophobic polycation immobilized surface) (Hsu et al., 2011), and spontaneous virion disassembly and physical disruption of the virion (Murray and Laband, 1979) that will influence virus inactivation. Consequently, differences in the depth of the primary minimum for viruses on heterogeneous surfaces may also explain the need to use separate solid phase inactivation rates in the two-site model.

Reversible and irreversible virus attachment is therefore highly sensitive to the chemical heterogeneity and roughness conditions on both the solid and virus surface. For example, irreversible virus attachment may occur at smooth surfaces with chemical heterogeneity due to the presence of deep primary minimum, whereas reversible virus interaction was expected on rough surfaces due to the presence of a shallow primary minimum (Bradford et al., 2017; Bradford and Torkzaban, 2012). This implies that only a very small fraction of the solid surface may contribute to irreversible virus attachment in a deep primary minimum since nanoscale roughness is ubiquitous on solid and virus surfaces (Bradford et al., 2017; Bradford and Torkzaban, 2015). These findings are consistent with the small values of α (0.028–0.081) and S_f (8.5×10^{-7}–7.8×10^{-9}) shown in Table 1, and the observed blocking behavior for both viruses in the BTCs (Fig. 1) and our previous study (Sasidharan et al., 2017a). An increase in temperature decreases the energy barrier height and increases the depth of the primary minimum (Sasidharan et al., 2017b). A slight increase in the depth of the primary minimum may increase the fraction of the surface that is favorable to irreversible attachment and may explain the increased retention and solid phase inactivation of viruses at a higher temperature.

Conclusions and Implications

Experimental results demonstrated that virus attachment increased with temperature, and 95% of the injected viruses were irreversibly retained on the solid surface. An advective–dispersive transport model with one-site attachment, detachment, blocking, and solid and liquid phase inactivation provided an adequate description of the initial BTC. Liquid phase inactivation had a negligible effect on observed virus BTCs compared with irreversible attachment and solid phase inactivation, i.e., $k_{att1} > \mu_{s1} >> \mu_l$. However, a two-site model was needed to accurately describe low levels of long-term virus release; i.e., $k_{att1} >> k_{att2}$, $\mu_{s1} >> \mu_{s2}$, and $k_{det1} > k_{det2}$. The calculated values of S_f and α were always very small, which implies that only a small fraction of the solid surface was favorable for attachment. This observation could be explained by the presence of nanoscale roughness on surfaces of viruses and sand, which decreases the energy barrier and depth of the primary minimum.

Although the vast majority of viruses were irreversibly retained on the solid phase, a small percentage (<4.17%) were released into flowing water, especially during transient solution chemistry conditions, which can pose a potential risk of long-term transport and to human health. However, the reversible virus fraction decreased with increasing temperature (4 to 20°C), increasing storage duration (0 to 70 d), and for ΦX174 in comparison to PRD1 due to increases in solid phase inactivation. In addition, temperature cycling (flow at 20°C and storage at 4°C) demonstrated that solid phase inactivation was a function of temperature.

Acknowledging irreversible attachment, solid phase inactivation, and liquid phase inactivation in MAR guidelines can significantly reduce the number of expensive treatments such as ultraviolet, reverse osmosis, and micro-membrane filtration. In particular, the risk of virus release during MAR can be minimized or eliminated by selecting an adequate residence time for

liquid and especially solid phase inactivation under expected groundwater flow and temperature conditions. For example, our long-term experimental results suggest that a 2 to 3 mo residence time will be sufficient to remove one to three logs of viruses via irreversible attachment and solid phase inactivation in aquifers with a temperature above 20°C. Note that the residence time for current MAR applications such as ASR and ASTR in Australia and United States is 6 to 9 mo when the winter storm is collected and recovered during summer (Donald et al., 2011; Kremer et al., 2008; NRMMC–EPHC–NHMRC, 2009; Rahman et al., 2012; Toze et al., 2010). However, the residence time may be shorter in the event of harvesting spring and summer storms. In some instances, cold stormwater may be injected into a warm groundwater. In this case, the time required for the mixing and equilibrium of both waters should be considered in the residence time calculation. This would be especially beneficial for the ASTR technique (e.g., injected water is mixed with the groundwater and transferred to the recovery well) because it would provide a greater opportunity for virus removal via solid phase attachment and inactivation.

Conducting laboratory-scale column experiments can help to gain a mechanistic understanding of the process and factors that control virus removal in saturated porous media. However, it is important to translate this knowledge to field-scale applications. Several column studies have demonstrated the importance of site-specific differences such as virus type, sediment mineralogy, injection water and groundwater composition, flow regimes, temperature, residence time, and native microbial community on virus removal in porous media. For example, metal oxides and calcite-rich sediments have been demonstrated to produce a three to four log removal of viruses via solid phase attachment and inactivation (Sasidharan et al., 2017a). The selection of potential MAR sites with favorable sediment mineralogy will therefore also play a key role in determining the efficacy of the ASTR applications. Conversely, one should be cautious about the potential health risk associated viruses with low inactivation rates, groundwater with low temperature, and aquifers with high permeability zones with low residence times.

Future MAR guidelines could be based on a database of column-scale and field-scale virus transport and fate experiments. Column-scale studies for site-specific conditions are relatively cheap and easy to conduct. Results from such column-scale studies could be used to aid the design of a limited number of field-scale experiments to validate whether an acceptable level of the virus removal can be achieved via ASR or ASTR techniques. Conducting several site-specific column and field-scale studies could lead to the development of a database of results for various geologic conditions to inform MAR guidelines. This information could be further extended through numerical modeling and calibration of pathogen retention and inactivation parameters.

Supplemental Material

The standard error coefficients for fitted parameters are given in Supplemental Table S1, available online.

Acknowledgments

The project was completed in collaboration with CSIRO Land and Water program and the Flinders University of South Australia. The experimental work was conducted in the CSIRO Laboratories at the Waite Campus, Adelaide, South Australia.

References

Adamczyk, Z., B. Siwek, M. Zembala, and P. Belouschek. 1994. Kinetics of localized adsorption of colloid particles. Adv. Colloid Interface Sci. 48:151–280.

Anders, R., and C.V. Chrysikopoulos. 2006. Evaluation of the factors controlling the time-dependent inactivation rate coefficients of bacteriophage MS2 and PRD1. Environ. Sci. Technol. 40(10):3237–3242. doi:10.1021/es051604b

Asano, T., and A.D. Levine. 1996. Wastewater reclamation, recycling and reuse: Past, present, and future. Water Sci. Technol. 33(10–11):1–14. doi:10.1016/0273-1223(96)00401-5

Blanc, R., and A. Nasser. 1996. Effect of effluent quality and temperature on the persistence of viruses in soil. Water Sci. Technol. 33:237–242. doi:10.1016/0273-1223(96)00425-8

Bradford, S.A., H. Kim, C. Shen, S. Sasidharan, and J. Shang. 2017. Contributions of nanoscale roughness to anomalous colloid retention and stability behavior. Langmuir 33(38):10094–10105. doi:10.1021/acs.langmuir.7b02445

Bradford, S.A., Y.F. Tadassa, and Y. Jin. Transport of coliphage in the presence and absence of manure suspension. J. Environ. Qual. 35 (2006) 1692–1701. doi:10.2134/jeq2006.0036

Bradford, S.A., and S. Torkzaban. 2012. Colloid adhesive parameters for chemically heterogeneous porous media. Langmuir 28(38):13643–13651. doi:10.1021/la3029929

Bradford, S.A., and S. Torkzaban. 2013. Colloid interaction energies for physically and chemically heterogeneous porous media. Langmuir 29(11):3668–3676. doi:10.1021/la400229f

Bradford, S.A., and S. Torkzaban. 2015. Determining parameters and mechanisms of colloid retention and release in porous media. Langmuir 31(44):12096–12105. doi:10.1021/acs.langmuir.5b03080

Choo, H., J. Larrahondo, and S.E. Burns. 2015. Coating effects of nano-sized particles on sand surfaces: Small strain stiffness and contact mode of iron oxide coated sands. J. Geotech. Geoenviron. Eng. 141(1):04014077. doi:10.1061/(ASCE)GT.1943-5606.0001188

Chrysikopoulos, C.V., and A.F. Aravantinou. 2012. Virus inactivation in the presence of quartz sand under static and dynamic batch conditions at different temperatures. J. Hazard. Mater. 233-234:148–157. doi:10.1016/j.jhazmat.2012.07.002

Chu, Y., Y. Jin, M. Flury, and M.V. Yates. 2001. Mechanisms of virus removal during transport in unsaturated porous media. Water Resour. Res. 37(2):253–263.

Dillon, P., S. Toze, D. Page, J. Vanderzalm, E. Bekele, J. Sidhu, and S. Rinck-Pfeiffer. 2010. Managed aquifer recharge: Rediscovering nature as a leading-edge technology. Water Sci. Technol. 62(10):2338–2345. doi:10.2166/wst.2010.444

Donald, M., K. Mengersen, S. Toze, J.P.S. Sidhu, and A. Cook. 2011. Incorporating parameter uncertainty into quantitative microbial risk assessment (QMRA). J. Water Health 9(1):10–26. doi:10.2166/wh.2010.073

Engström, M., and B. Nordell. 2016. Temperature-driven groundwater convection in cold climates. Hydrogeol. J. 24(5):1245–1253. doi:10.1007/s10040-016-1420-0

Gordon, C., and S. Toze. 2003. Influence of groundwater characteristics on the survival of enteric viruses. J. Appl. Microbiol. 95(3):536–544. doi:10.1046/j.1365-2672.2003.02010.x

Gunawardhana, L., K. So, and S. Masaki. 2009. Seasonal change of groundwater flow and its effect on temperature distribution in Sendai plain. In: C. Zhang and H. Tang, editors, Advances in water resources and hydraulic engineering. Springer, Berlin. p. 193–198. doi:10.1007/978-3-540-89465-0_36

Han, Y., G. Hwang, D. Kim, S.A. Bradford, B. Lee, I. Eom, P.J. Kim, S.Q. Choi, and H. Kim. 2016. Transport, retention, and long-term release behavior of ZnO nanoparticle aggregates in saturated quartz sand: Role of solution pH and biofilm coating. Water Res. 90:247–257. doi:10.1016/j.watres.2015.12.009

Hannappel, S., F. Scheibler, A. Huber, and C. Sprenger. 2014. Application of the Australian guidelines for water recycling: Managing health and environmental risk. European Community's Seventh Framework Programme under Grant Agreement No. 308339 (Project DEMEAU). http://demeau-fp7.eu/results/mar.

Harvey, R.W., and J.N. Ryan. 2004. Use of PRD1 bacteriophage in groundwater viral transport, inactivation, and attachment studies. FEMS Microbiol. Ecol. 49(1):3–16. doi:10.1016/j.femsec.2003.09.015

Hijnen, W.A., A.J. Brouwer-Hanzens, K.J. Charles, and G.J. Medema. 2005. Transport of MS2 phage, *Escherichia coli*, *Clostridium perfringens*, *Cryptosporidium parvum*, and *Giardia intestinalis* in a gravel and a sandy soil. Environ. Sci. Technol. Lett. 39(20):7860–7868. doi:10.1021/es050427b

Hsu, B.B., S.Y. Wong, P.T. Hammond, J. Chen, and A.M. Klibanov. 2011. Mechanism of inactivation of influenza viruses by immobilized hydrophobic polycations. Proc. Natl. Acad. Sci. USA 108(1):61–66. doi:10.1073/pnas.1017012108

ISO. 2000. ISO 10705-2-2000: Water quality—Detection and enumeration of bacteriophages—Part 2: Enumeration of somatic coliphages. International Organization for Standardization, Geneva.

Jansons, J., L.W. Edmonds, B. Speight, and M.R. Bucens. 1989. Survival of viruses in groundwater. Water Res. 23(3):301–306. doi:10.1016/0043-1354(89)90095-X

Johnson, I. 1989. Artificial recharge of ground water. Environ. Geol. (Denver Colo.) 14(3):157–158.

Johnson, P.R., and M. Elimelech. 1995. Dynamics of colloid deposition in porous media: Blocking based on random sequential adsorption. Langmuir 11(3):801–812. doi:10.1021/la00003a023

Katzenelson, E. 1978In: Berg, G., editor, Survival of viruses. Indicators of viruses in water and food. Ann Arbor Science, Ann Arbor, MI.

Kazumori, Y. 1981. Electron microscopic studies of bacteriophage φ X174 intact and 'eclipsing' particles, and the genome by the staining and shadowing method. J. Virol. Methods 2(3):159–167. doi:10.1016/0166-0934(81)90034-3

Keswick, B.H., C.P. Gerba, S.L. Secor, and I. Cech. 1982. Survival of enteric viruses and indicator bacteria in groundwater. J. Environ. Sci. Health Part A 17(6):903–912. doi:10.1080/10934528209375085

Kim, H.N., S.A. Bradford, and S.L. Walker. 2009. *Escherichia coli* O157: H7 transport in saturated porous media: Role of solution chemistry and surface macromolecules. Environ. Sci. Technol. 43(12):4340–4347. doi:10.1021/es8026055

Kremer, S., P. Pavelic, P. Dillon, and K. Barry. 2008. Flow and solute transport observations and modelling from the first phase of flushing operations at the Salisbury ASTR site. CSIRO, Water for a Healthy Country National Research Flagship, Canberra, Australia.

Liew, P., and C.P. Gerba. 1980. Thermostabilization of enteroviruses by estuarine sediment. Appl. Environ. Microbiol. 40(2):305–308.

McKenna, R., D. Xia, P. Willingmann, L.L. Ilag, S. Krishnaswamy, M.G. Rossmann, N.H. Olson, T.S. Baker, and N.L. Incardona. 1992. Atomic structure of single-stranded DNA bacteriophage φX174 and its functional implications. Nature 355(6356):137–143. doi:10.1038/355137a0

Merckel, M.C., J.T. Huiskonen, D.H. Bamford, A. Goldman, and R. Tuma. 2005. The structure of the bacteriophage PRD1 spike sheds light on the evolution of viral capsid architecture. Mol. Cell 18(2):161–170. doi:10.1016/j.molcel.2005.03.019

Messina, F., D.L. Marchisio, and R. Sethi. 2015. An extended and total flux normalized correlation equation for predicting single-collector efficiency. J. Colloid Interface Sci. 446:185–193. doi:10.1016/j.jcis.2015.01.024

Mondon, M., S. Berger, and C. Ziegler. 2003. Scanning-force techniques to monitor time-dependent changes in topography and adhesion force of proteins on surfaces. Anal. Bioanal. Chem. 375(7):849–855. doi:10.1007/s00216-003-1751-2

Murray, J.P., and S.J. Laband. 1979. Degradation of poliovirus by adsorption on inorganic surfaces. Appl. Environ. Microbiol. 37(3):480–486.

NHMRC. 2011. Australian drinking water guidelines 6: National water quality management strategy. National Health and Medical Research Council, Natural Resource Management Ministerial Council, Commonwealth of Australia, Canberra.

NRMMC–EPHC–NHMRC. 2009. Australian guidelines for water recycling: Managing health and environmental risks (phase 2)—Managed aquifer recharge. National Water Quality Management Strategy. Natural Resource Ministerial Management Council, Environment Protection and Heritage Council, and National Health and Medical Research Council. Canberra, Australia. http://www.nepc.gov.au/system/files/resources/5fe5174a-bdec-a194-79ad-86586fd19601/files/wq-agwr-gl-managed-aquifer-recharge-final-200907_1.pdf.

Page, D., D. Gonzalez, and P. Dillon. 2012. Microbiological risks of recycling urban stormwater via aquifers. Water Sci. Technol. 65(9):1692–1695. doi:10.2166/wst.2012.069

Page, D.W., J.L. Vanderzalm, K.E. Barry, S. Torkzaban, D. Gonzalez, and P.J. Dillon. 2015. *E. coli* and turbidity attenuation during urban stormwater recycling via aquifer storage and recovery in a brackish limestone aquifer. Ecol. Eng. 84:427–434. doi:10.1016/j.ecoleng.2015.09.023

Peralta, B., D. Gil-Carton, D. Castaño-Díez, A. Bertin, C. Boulogne, H.M. Oksanen, D.H. Bamford, and N.G.A. Abrescia. 2013. Mechanism of membranous tunnelling nanotube formation in viral genome delivery. PLoS Biol. 11:e1001667.

Pieper, A.P., J.N. Ryan, R.W. Harvey, G.L. Amy, T.H. Illangasekare, and D.W. Metge. 1997. Transport and recovery of bacteriophage PRD1 in a sand and gravel aquifer: Effect of sewage-derived organic matter. Environ. Sci. Technol. 31(4):1163–1170. doi:10.1021/es960670y

Rahman, M.A., B. Rusteberg, R.C. Gogu, J.P. Lobo Ferreira, and M. Sauter. 2012. A new spatial multi-criteria decision support tool for site selection for implementation of managed aquifer recharge. J. Environ. Manage. 99 (Supplement C):61–75. doi:10.1016/j.jenvman.2012.01.003

Reynolds, K.A., K.D. Mena, and C.P. Gerba. 2008. Risk of waterborne illness via drinking water in the United States. In: D.M. Whitacre, editor, Reviews of environmental contamination and toxicology. Springer, New York. p. 117–158.

Ryan, J.N., R.W. Harvey, D. Metge, M. Elimelech, T. Navigato, and A.P. Pieper. 2002. Field and laboratory investigations of inactivation of viruses (PRD1 and MS2) attached to iron oxide-coated quartz sand. Environ. Sci. Technol. 36(11):2403–2413. doi:10.1021/es011285y

Sasidharan, S., S.A. Bradford, J. Šimůnek, S. Torkzaban, and J. Vanderzalm. 2017a. Transport and fate of viruses in sediment and stormwater from a managed aquifer recharge site. J. Hydrol. 555 (Supplement C): 724–735. doi:10.1016/j.jhydrol.2017.10.062

Sasidharan, S., S. Torkzaban, S.A. Bradford, P.G. Cook, and V.V. Gupta. 2017b. Temperature dependency of virus and nanoparticle transport and retention in saturated porous media. J. Contam. Hydrol. 196:10–20. doi:10.1016/j.jconhyd.2016.11.004

Sasidharan, S., S. Torkzaban, S.A. Bradford, P.J. Dillon, and P.G. Cook. 2014. Coupled effects of hydrodynamic and solution chemistry on long-term nanoparticle transport and deposition in saturated porous media. Colloids Surf. A Physicochem. Eng. Asp. 457(5):169–179. doi:10.1016/j.colsurfa.2014.05.075

Sasidharan, S., S. Torkzaban, S.A. Bradford, R. Kookana, D. Page, and P.G. Cook. 2016. Transport and retention of bacteria and viruses in biochar-amended sand. Sci. Total Environ. 548–549:100–109. doi:10.1016/j.scitotenv.2015.12.126

Schijven, J.F., and S.M. Hassanizadeh. 2000. Removal of viruses by soil passage: Overview of modeling, processes, and parameters. Crit. Rev. Environ. Sci. Technol. 30(1):49–127. doi:10.1080/10643380091184174

Schijven, J.F., S.M. Hassanizadeh, and R.H.A.M. De Bruin. 2002. Two-site kinetic modeling of bacteriophages transport through columns of saturated dune sand. J. Contam. Hydrol. 57(3-4):259–279. doi:10.1016/S0169-7722(01)00215-7

Schijven, J.F., W. Hoogenboezem, M. Hassanizadeh, and J.H. Peters. 1999. Modeling removal of bacteriophages MS2 and PRD1 by dune recharge at Castricum, Netherlands. Water Resour. Res. 35(4):1101–1111.

Schijven, J.F., G. Sadeghi, and S.M. Hassanizadeh. 2016. Long-term inactivation of bacteriophage PRD1 as a function of temperature, pH, sodium and calcium concentration. Water Res. 103:66–73. doi:10.1016/j.watres.2016.07.010

Schmoll, O. 2006. Protecting groundwater for health: Managing the quality of drinking-water sources. IWA Publishing, London.

Sidhu, J. P. S., S. Toze, L. Hodgers, K. Barry, D. Page, Y. Li, and P. Dillon. 2015. Pathogen decay during managed aquifer recharge at four sites with different geochemical characteristics and recharge water sources. J. Environ. Qual. 44: 1402–1412. doi:10.2134/jeq2015.03.0118

Sidhu, J.P.S., S. Toze, L. Hodgers, M. Shackelton, K. Barry, D. Page, and P. Dillon. 2010. Pathogen inactivation during passage of stormwater through a constructed reedbed and aquifer transfer, storage, and recovery. Water Sci. Technol. 62(5):1190–1197. doi:10.2166/wst.2010.398

Sim, Y., and C.V. Chrysikopoulos. 1996. One-dimensional virus transport in porous media with time-dependent inactivation rate coefficients. Water Resour. Res. 32(8):2607–2611. doi:10.1029/96WR01496

Šimůnek, J., M.T. van Genuchten, and M. Sejna. 2016. Recent developments and applications of the HYDRUS computer software packages. Vadose Zone J. 15(7). doi:10.2136/vzj2016.04.0033

Stagg, C.H., C. Wallis, and C.H. Ward. 1977. Inactivation of clay-associated bacteriophage MS-2 by chlorine. Appl. Environ. Microbiol. 33(2):385–391.

Stuart, J.K., and V. Hlady. 1995. Effects of discrete protein-surface interactions in scanning force microscopy adhesion force measurements. Langmuir 11(4):1368–1374. doi:10.1021/la00004a051

Torkzaban, S., and S.A. Bradford. 2016. Critical role of surface roughness on colloid retention and release in porous media. Water Res. 88:274–284. doi:10.1016/j.watres.2015.10.022

Toze, S., E. Bekele, D. Page, J. Sidhu, and M. Shackleton. 2010. Use of static quantitative microbial risk assessment to determine pathogen risks in an unconfined carbonate aquifer used for managed aquifer recharge. Water Res. 44(4):1038–1049. doi:10.1016/j.watres.2009.08.028

Vadillo-Rodríguez, V., H.J. Busscher, W. Norde, J. de Vries, and H.C. van der Mei. 2004. Atomic force microscopic corroboration of bond aging for adhesion of *Streptococcus thermophilus* to solid substrata. J. Colloid Interface Sci. 278(1):251–254. doi:10.1016/j.jcis.2004.05.045

van Leeuwen, J.H. 1996. Reclaimed water—an untapped resource. Desalination 106(1–3):233–240. doi:10.1016/0011-9164(96)00113-0

Walker, S.L., J.A. Redman, and M. Elimelech. 2004. role of cell surface lipopolysaccharides in *Escherichia coli* K12 adhesion and transport. Langmuir 20(18):7736–7746. doi:10.1021/la049511f

Xu, L.-C., and B.E. Logan. 2006. Adhesion forces between functionalized latex microspheres and protein-coated surfaces evaluated using colloid probe atomic force microscopy. Colloids Surf. B Biointerfaces 48(1):84–94. doi:10.1016/j.colsurfb.2006.01.012

Yao, K.-M., M.T. Habibian, and C.R. O'Melia. 1971. Water and wastewater filtration: Concepts and applications. Environ. Sci. Technol. 5(11):1105–1112. doi:10.1021/es60058a005

Yates, M.V., S.R. Yates, and C.P. Gerba. 1988. Modeling microbial fate in the subsurface environment. Crit. Rev. Environ. Sci. Technol. 17(4):307–344.

Zhang, W., V.L. Morales, M.E. Cakmak, A.E. Salvucci, L.D. Geohring, A.G. Hay, J.Y. Parlange, and T.S. Steenhuis. 2010. Colloid transport and retention in unsaturated porous media: Effect of colloid input concentration. Environ. Sci. Technol. 44(13):4965–4972. doi:10.1021/es100272f

SUPPORTING INFORMATION

Minimizing Virus Transport in Porous Media by Optimizing Solid Phase Inactivation

Salini Sasidharan[1,2,3*], Scott A. Bradford[4], Jiří Šimůnek[1], and Saeed Torkzaban[3]

[1]Department of Environmental Sciences, University of California Riverside, Riverside, CA 92521, USA

[2]CSIRO Land and Water, Glen Osmond, SA 5064, Australia

[3]Flinders University, Adelaide, SA 5001, Australia

[4]USDA, ARS, U. S. Salinity Laboratory, Riverside, CA 92507, USA

Table: S1

*Corresponding Author
Salini Sasidharan
Phone: +951-369-4805
Email: salinis@ucr.edu

Table S1: The standard error coefficient (*S.E Coeff*) for fitted model parameters k_{att1}, S_{max1}, k_{det1}, μ_{s1}, k_{att2}, and k_{det2} to viruses PRD1 and ΦX174 BTCs using one-site or two-site kinetic models. The simulated BTCs shown in Figure 1B and the corresponding fitted model parameters are given in Table 1.

Virus	Temperature	Model	*S.E Coeff* - k_{att1}	*S.E Coeff* – S_{max1}	*S.E Coeff* – k_{det1}	*S.E Coeff* – μ_{s1}	*S.E Coeff* – k_{att2}	*S.E Coeff* – k_{det2}
	[°C]							
ΦX174	4	One-Site	9.3×10^{-3}	5.9×10^{-1}	1.7×10^{-4}	3.4×10^{-3}	NA	NA
		Two-Site	5.0×10^{-3}	NA	NA	NA	1.6×10^{-6}	3.3×10^{-6}
	20	One-Site	1.4×10^{-2}	5.36	1.8×10^{-3}	1.0×10^{-3}	NA	NA
		Two-Site	5.9×10^{-3}	NA	NA	NA	1.3×10^{-6}	1.9×10^{-5}
PRD1	4	One-Site	9.3×10^{-3}	1.9×10^{-1}	4.2×10^{-3}	1.9×10^{-4}	NA	NA
		Two-Site	7.1×10^{-3}	NA	NA	NA	6.6×10^{-7}	1.1×10^{-5}
	20	One-Site	6.5×10^{-3}	6.1×10^{-1}	5.5×10^{-8}	3.0×10^{-5}	NA	NA
		Two-Site	5.0×10^{-1}	NA	NA	N A	1.6×10^{-9}	4.7×10^{-4}